PCCP

Transition-State Correlations for Predicting Thermochemistry of Adsorbates and Surface Reactions

Journal:	*Physical Chemistry Chemical Physics*
Manuscript ID	CP-ART-09-2022-004425.R1
Article Type:	Paper
Date Submitted by the Author:	04-Jan-2023
Complete List of Authors:	Kurdziel, Sophia; University of Delaware, Department of Chemical and Biomolecular Engineering Vlachos, Dionisios; Univ. of Delaware,

Transition-State Correlations for Predicting Thermochemistry of Adsorbates and Surface Reactions

Sophia J. Kurdziel[1] and Dionisios G. Vlachos[1,2]*

[1]*Department of Chemical and Biomolecular Engineering, University of Delaware, 150 Academy Street, Newark, DE 19716*

[2]*Catalysis Center for Energy Innovation, RAPID Manufacturing Institute, Delaware Energy Institute (DEI), University of Delaware, 221 Academy Street, Newark, DE 19716*

*Corresponding author: **vlachos@udel.edu*

Abstract

Estimating thermochemical properties from linear correlations may provide a pathway to circumvent expensive density functional theory (DFT) calculations for quantities such as pre-exponentials and temperature corrections to DFT energies. Here, we construct thermochemical scaling relations between C_1-C_6 *n*-alkanes in the gas phase and adsorbed alkyl chains extending from several transition metal surfaces, and examine changes in slope and fit between metals and adsorption sites. We subsequently add -OH, -NH_2, C=O, and C=C functional groups to the C_1-C_6 molecules and demonstrate strong linear correlations for thermochemistry across all species. We broaden the correlations to incorporate transition states of C_1-C_6 *n*-alkane dehydrogenation reactions, where thermochemistry for computationally prohibitive transition-state calculations can be quickly assessed. Additionally, we rationalize the linearity of thermochemical correlations based on the composition of the homologous series and theoretical assessments. As an application of the correlations, we estimate pre-exponentials for elementary surface reactions of ethane and propane hydrogenolysis on Ru(0001), which is of relevance to plastics hydrogenolysis. Depending on kinetically important steps, entropic contributions may be necessary to include in certain reactions mechanisms; in contrasting examples, entropies are found to be relatively insignificant for ethane hydrogenolysis but pertinent for propane hydrogenolysis.

Introduction

Simulation of heterogeneous catalytic reactions often involves (semi)-empirical estimation of properties such as electronic energies,[1,2,3] vibrational frequencies,[4,5,6] and thermochemical quantities[5-7] otherwise computationally demanding to calculate from first-principles. Linear correlations, such as transition-state scaling (TSS) and Brønsted-Evans-Polanyi (BEP) relations,[2] are well-established for electronic energies and are used routinely to avoid arduous density functional theory (DFT) calculations. In the case of the TSS/BEP, local minimum energetics are used to estimate transition state (TS) energies or activation barriers, respectively. Beyond energy scaling, Campbell and Sellers demonstrated that experimentally-determined entropies of molecular adsorbates and gas-phase species correlate for adsorption and/or desorption on two-dimensional (2D) catalytic surfaces.[7,8] Adsorbate entropies were found to be approximately 2/3 of the corresponding gas-phase species, generalized to the loss of a translational degree of freedom perpendicular to the surface. Over a range of species, the measured entropies were well-fit to a single linear regression; the relationship was found to be nearly independent of

the molecule with discernible yet minimal variation in the slope and *y*-intercept among surfaces and sites. Proceeding studies have found the linear dependence between gas-phase and adsorbed entropies measured by experiment or simulation holds for chemically diverse datasets, including small organic molecules on 2D mineral surfaces,[9] and species confined in zeolite adsorbents.[10,11] Adsorption enthalpies and entropies have also been shown to linearly correlate for *n*-alkane species confined in zeolites.[12] The linear relations of Campbell and Sellers enabled reliable estimations of pre-exponentials for adsorption/desorption steps, but beyond this, entropic correlations have not incorporated TSs.

In microkinetic modeling of heterogeneous catalytic systems, pre-exponential factors are often taken as a constant ($\frac{k_b T}{h}$, where k_b is Boltzmann's constant, T is temperature, and h is Planck's constant) approximated from TS theory, neglecting entropic differences between initial states (ISs) and TSs for elementary surface reactions.[13-15] Alternatively, classification of elementary reaction steps into families had reduced the complexity of mechanistic simulations;[16] specifically, a single pre-exponential across an entire homologous series has been assumed,[17] but the validity of the approximation has not been assessed. Similarly to estimating activation barriers using BEP relations, thermochemical scaling between gas-phase species or ISs and their TSs of bond-breaking or forming reactions may prove especially useful for avoiding expensive DFT calculations. For AH_X (A = C, N, O) diffusion/dehydrogenation reactions on transition metal surfaces, the concept of linearly correlating individual metal-adsorbate driven modes between local minima and transition states was extended to thermochemical properties calculated from vibrational frequencies, and demonstrated across metal surfaces and the AH_X homologous series.[4,5,6] Additionally, for larger molecules DFT computations become especially prohibitive; estimating surface species thermochemical properties from linearly correlated gas-phase or local minimum data, whether from performing the lower-effort calculation only or obtaining pertinent data from repositories, should save substantial computational time and effort. Vibrational contributions for surface reactions can be easily obtained, where one can gauge pre-exponentials for rate constants, zero-point energy contributions, and temperature corrections to electronic energies.

Here, using DFT we first demonstrate the existence of linear thermochemical correlations between gas-phase *n*-alkanes and dehydrogenated alkyl chains adsorbed on a single surface site of fcc(111) transition metals, and subsequently add functional groups to examine changes in slope and fit. We then develop thermochemical scaling between gas-phase species and the TSs of dehydrogenation reactions, and compare computational and experimental references for gas-phase species. We elaborate on frequency shifting between different modes on transition metal surfaces, and offer theoretical insight into the driving forces behind thermochemical correlations. Additionally, we incorporate thermochemical scaling relationships between ISs and TSs of elementary reactions into microkinetic models for both propane and ethane hydrogenolysis on Ru(0001), where we parametrize the pre-exponential and examine the effects of entropic contributions on kinetically relevant steps.

Methods

Density Functional Theory (DFT) Calculations

Electronic energies and vibrational frequencies were calculated for gas-phase *n*-alkanes (C_1-C_6) and corresponding dehydrogenated alkyl chains (C_1-C_6) at atop sites for platinum (Pt) and rhodium (Rh) surfaces and fcc hollow sites for copper (Cu) and nickel (Ni) fcc(111) surfaces. Additional functional groups were then incorporated on the Pt(111) surface, including -OH, -NH_2, C=O, and C=C. All species and surface combinations are listed in Tables S1 and S2 of the Supporting Information (SI). Periodic DFT calculations were performed using the Vienna Ab initio Simulation Package (VASP)[18] version 5.4.1 and

inputs were generated using the Atomic Simulation Environment (ASE).[19] The revised Perdew-Burke-Ernzerhof (RPBE) density functional[20] with D3 dispersion corrections[21] was used to describe exchange and correlation energies of electrons. The projector augmented wave (PAW) method was employed to describe core electrons,[22] while valence electrons were represented with a plane wave basis. A plane wave cutoff of 400 eV was used for surface calculations, and self-consistent energies were converged to 10^{-5} eV. Brillouin zone integration for slab calculations was done with a gamma-centered 5x5x1 Monkhorst−Pack *k*-point mesh.[23] Spin-polarized calculations were performed for gas-phase molecules and Ni(111) surfaces. Gas-phase calculations were performed inside 25x25x25 Å supercells with Brillouin zone integration at the gamma point only and a 0.005 eV/Å force cutoff.

Unit Cell Setup

Bulk metal structures were obtained from the American Mineralogical Crystal Structure Database.[24] To simulate the bulk, lattice constants were calculated using the tetrahedron method with Blöchl corrections, an 11x11x11 Monkhorst−Pack grid, and a 520 eV plane wave cutoff energy. The lattice constants were optimized until forces converged at 0.01 eV/Å. A four-layer 4x4 slab where the top two layers were allowed to relax and the bottom two layers were frozen was used to model the fcc(111) transition metal surfaces. A vacuum of 20 Å and dipole corrections perpendicular to the surface were added to avoid interaction between periodic images for slab calculations, and all forces were minimized to below 0.03 eV/Å for geometry optimizations. The first order Methfessel-Paxton method was used with a smearing width of 0.2 eV.

Transition State (TS) and Thermochemical Calculations

For TS calculations, local minima and intermediate images were modeled using a four-layer 5x5 slab with the bottom two layers fixed, and the Brillouin zone was sampled with a gamma-centered 7x7x1 *k*-point mesh. The TS geometries were found using the nudged elastic band (NEB) method following by the climbing-image or dimer method.[25,26] A single imaginary frequency was verified for all TS calculations.

Vibrational modes were determined from the eigenvalues of the Hessian matrix, with 0.005 or 0.015 Å displacements from equilibrium positions in the *x*, *y*, and *z* directions for all atoms in the molecule. Surface atoms were held fixed for vibrational frequency calculations. In a few cases for adsorbed species, one small (< 50*i* cm^{-1}) imaginary frequency was present in vibrational mode calculations even with stricter convergence criteria for geometry optimizations (self-consistent energies = 10^{-8} eV, force cutoff = 0.01 eV/Å). The imaginary frequency was replaced with a value of 20 cm^{-1} to obtain the harmonic thermochemistry.[27] We note these in the SI. In the harmonic approximation, translational, rotational, and vibrational entropies are calculated[28] via Equations 1-3, and gas-phase entropies are determined from the sum of these components (Equation 4):

$$\frac{S_{trans}}{R} = \left[\frac{3}{2} ln\left(\frac{2\pi m}{h^2}\right) + \frac{5}{2} ln(k_B T) - ln(p) + \frac{5}{2}\right], \quad 1$$

$$\frac{S_{rot}}{R} = \left[ln\left(\frac{8\pi^2}{\sigma}\right) + \frac{3}{2} ln\left(\frac{2\pi k_B T}{h^2}\right) + \left(\frac{1}{2} ln(I_A I_B I_C)\right) + \frac{3}{2}\right], \quad 2$$

$$\frac{S_{vib}}{R} = \sum_i \left[\frac{h\nu_i}{k_B T\left(e^{\frac{h\nu_i}{k_B T}} - 1\right)} - ln\left(1 - e^{\frac{-h\nu_i}{k_B T}}\right)\right], \quad 3$$

$$S_{gas} = S_{trans} + S_{rot} + S_{vib}, \quad (4)$$

and similarly for computing zero-point energy (ZPE) and thermal corrections to electronic energies:

$$\frac{H_{trans}}{RT} = \frac{5}{2}, \quad (5)$$

$$\frac{H_{rot}}{RT} = \frac{3}{2}, \quad (6)$$

$$\frac{H_{vib}}{RT} = \sum_i \left[\frac{h\nu_i}{k_B T} \left(\frac{1}{2} + \frac{e^{\frac{-h\nu_i}{k_B T}}}{1 - e^{\frac{-h\nu_i}{k_B T}}} \right) \right], \quad (7)$$

$$H_{gas}^{corr} = H_{trans} + H_{rot} + H_{vib}. \quad (8)$$

For S_{trans}, m is the molar mass of the compound, h is Planck's constant, k_B is Boltzmann's constant, T is temperature, p is pressure, and R is the gas constant. For S_{rot}, other terms include σ, the symmetry number, and $I_A I_B I_C$, the product of the rotational moments of inertia. Symmetry numbers and rotational moments of inertia were obtained from NIST for gas-phase species.[29] H_{trans} and H_{rot} are constants at a given temperature. For S_{vib} and H_{vib}, calculations were performed as a summation over the number of vibrational degrees of freedom for every frequency ν_i. There are 3*N*-6 vibrational degrees of freedom for non-linear gas-phase species and 3*N* vibrational degrees of freedom for adsorbed species, where *N* is the number of atoms in the molecule. For first-order saddle points of dehydrogenations on surfaces, there are 3*N*-1 vibrational degrees of freedom. For the quasi-rigid rotor harmonic oscillator (qRRHO) model, the methods proposed by Grimme[30] and Head-Gordon[31] were used to continuously interpolate between rotational and vibrational thermochemical contributions, where the cutoff vibration is 100 cm^{-1}. For thermochemical contributions to the Gibbs energy:

$$\frac{G^{corr}}{RT} = \frac{H^{corr}}{RT} - \frac{S}{R}, \quad (9)$$

and besides adsorption from the gas phase, the rate constants of all elementary surface reactions were modeled using transition state theory:

$$k = \frac{k_b T}{h} exp\left(-\frac{\Delta G^{\ddagger}}{RT} \right) \quad (10)$$

where $\Delta G^{\ddagger}$ is the Gibbs free energy of activation.

Microkinetic Modeling (MKM) for Propane and Ethane Hydrogenolysis

Published data was used to obtain reaction networks and MKM conditions for propane and ethane hydrogenolysis on Ru(0001).[32] DFT data was either obtained from our internal database or supplemented with calculations using the same criteria as described in Reference 32. MKM simulations were performed in Chemkin.[33] DFT data was available for all elementary steps in the ethane hydrogenolysis model, while DFT data for propane hydrogenolysis was available for the kinetically important species and reactions.

Results and Discussion

Thermochemical Scaling Relationships for Adsorbates and Transition States of Surface Reactions

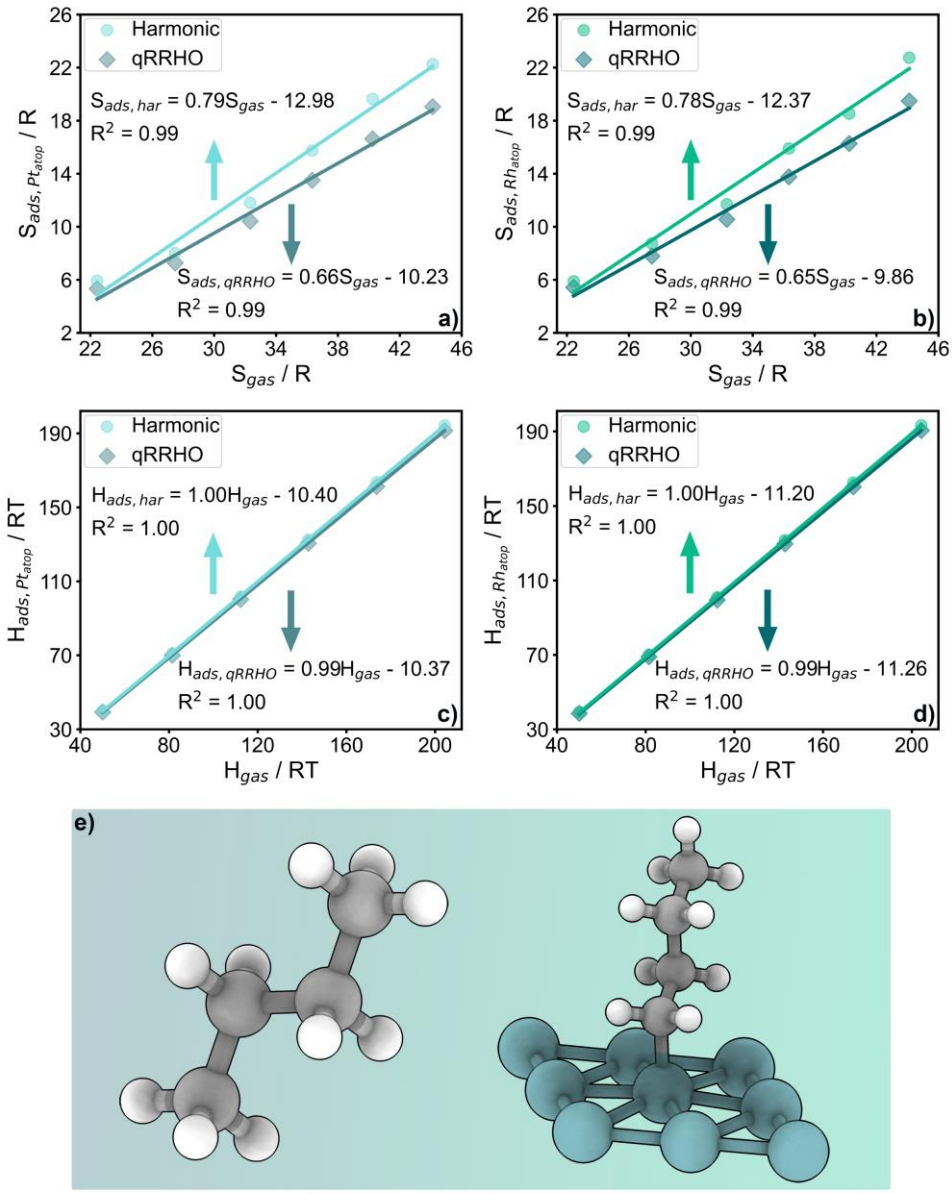

Figure 1. Thermochemical scaling of C_1-C_6 alkyls adsorbed on atop sites of Pt(111) **(a, c)** and Rh(111) **(b, d)** against gas-phase C_1-C_6 alkanes. Entropic **(a-b)** and enthalpic **(c-d)** contributions for adsorbed species (S_{ads}, H_{ads}) are calculated using the harmonic oscillator (circles) or the quasi-rigid rotor harmonic oscillator (qRRHO) model (diamonds). All thermochemistry is computed at 298.15 K. **(e)** Visual of a *n*-butane molecule in the gas-phase (left) and the corresponding butyl adsorbate on an atop site (right). Grey spheres denote carbon atoms, white spheres denote hydrogen atoms, and teal spheres denote metal atoms. Slopes, y-intercepts, and fits are rounded to two decimal places for brevity.

Thermochemical scaling relationships are first constructed between gas-phase (*n*-alkanes) and adsorbed (alkyl chains) species as shown in Figure 1. Using gas-phase data to estimate adsorbate contributions is particularly advantageous, given the low computational cost for such calculations and robust thermochemistry availability in databases. For gas-phase species, entropic and enthalpic corrections are calculated from the sum of vibrational, translational, and rotational contributions. Note that for the enthalpic corrections, translational and rotational partition functions are constants at a given temperature, and vibrational contributions are calculated with ZPE terms. For surface species, using the harmonic oscillator model all degrees of freedom are assumed to be vibrational, and for the qRRHO model, low-frequency modes are instead replaced with rotational contributions.[30] Typically, as the size of the gas-phase and adsorbed molecules increases, thermochemical contributions increase. This is generally intuitive, given the vibrational degrees of freedom increase with increasing species size. For gas-phase species, the translational and rotational contributions to the entropy also increase with molecule size. Figure 1 shows strong linear correlations between gas and adsorbed species for both harmonic and qRRHO approximations. Replacement of low-frequency vibrations ($\nu \rightarrow 0$) with rotational contributions will most prominently affect the slopes of entropic scaling; differences between harmonic and qRRHO models are visibly pronounced for entropic scaling compared to enthalpic scaling, especially as the size of the molecule increases. Thermochemical correlations constructed on the atop site are quite similar in slope and fit between Pt(111) and Rh(111). Figure S1 in the SI shows thermochemical scaling across fcc hollow sites for a hybrid of Cu(111) and Ni(111) data, demonstrating somewhat greater variation in the slope of entropic correlations compared to the relations constructed on atop sites, while enthalpic scaling maintains a similar regression to the atop site data. Apart from the linear regressions, differences in the numerical values of the thermochemistry across surfaces and sites may be partly attributed to mode shifting for alkyl chains. For example, the enthalpic contributions across atop sites are all slightly higher (on average ~1.3 RT) than those calculated in fcc hollow sites for both harmonic and qRRHO models. As intuition may suggest, modes attributed to direct interaction between the metal and adsorbate change depending on the surface and site, i.e. on a Pt versus Cu surface or on an atop versus hollow site. Previous work has sought to establish scaling relationships across transition metals based on these modes; for example, perpendicular modes classified based on *z* displacements between the metal surfaces and adsorbate, and parallel modes classified based on *x* or *y* displacements.[4] Additionally, mode softening, or significant shifting to a lower frequency on surfaces compared to gas-phase vibrations, occurs for molecular vibrations not directly related to interactions between the metal and monoatomic adsorbate. For example, the CH symmetric stretch vibration is likely softened at hollow sites because of shorter H-metal distances, allowing for the CH bonds of the nearest CH group to interact with the underlying surface. The CH bond becomes lengthened and weakened, and a mixing of CH bonding orbitals with *d* states of the metal surface takes place.[34] When the alkyl chain is adsorbed at atop sites, H-metal distances are longer and the CH-metal interaction is weaker. Thus, CH bonds at atop sites are only slightly stretched and experience a much smaller frequency shift.[34] Consequently, lower molecular vibrations due to frequency shifting contribute to comparatively smaller enthalpic terms, as seen for Cu(111) and Ni(111) adsorbates. Ultimately, the similarity between all regressions likely denotes the construction of the homologous series (*n*-alkanes/alkyl chains) drives the linear relations.

Functional groups, such as -OH, -NH_2, C=O, and C=C, are added the C_1-C_6 hydrocarbons in the gas phase and on Pt(111) atop sites. The resulting thermochemical correlations still hold for both harmonic and qRRHO models as shown in Figure S2 of the SI. The fits of the regressions degrade slightly for entropic scaling, but show little change for enthalpic contributions. This may be indicative of the sensitivity of entropies to the adsorbate, and may also be driven by the significant differences in enthalpic contributions among successively larger chain length (or increasing carbon number). Notably, the slopes of the qRRHO

scaling relations in Figures 1, S1, and S2 are similar to those of the entropic correlations developed by Campbell and Sellers.[7] The approach used in this work correlates DFT-computed properties of gas-phase and dehydrogenated species, and the ratios of adsorbate:gas-phase entropies are lower compared to the experimentally-derived correlations by Campbell and Sellers. Again, the similarity in slopes of the entropic scaling relationships may be dependent on the construction of the (successively increasing) homologous series, which is further examined through fundamental aspects later in this work.

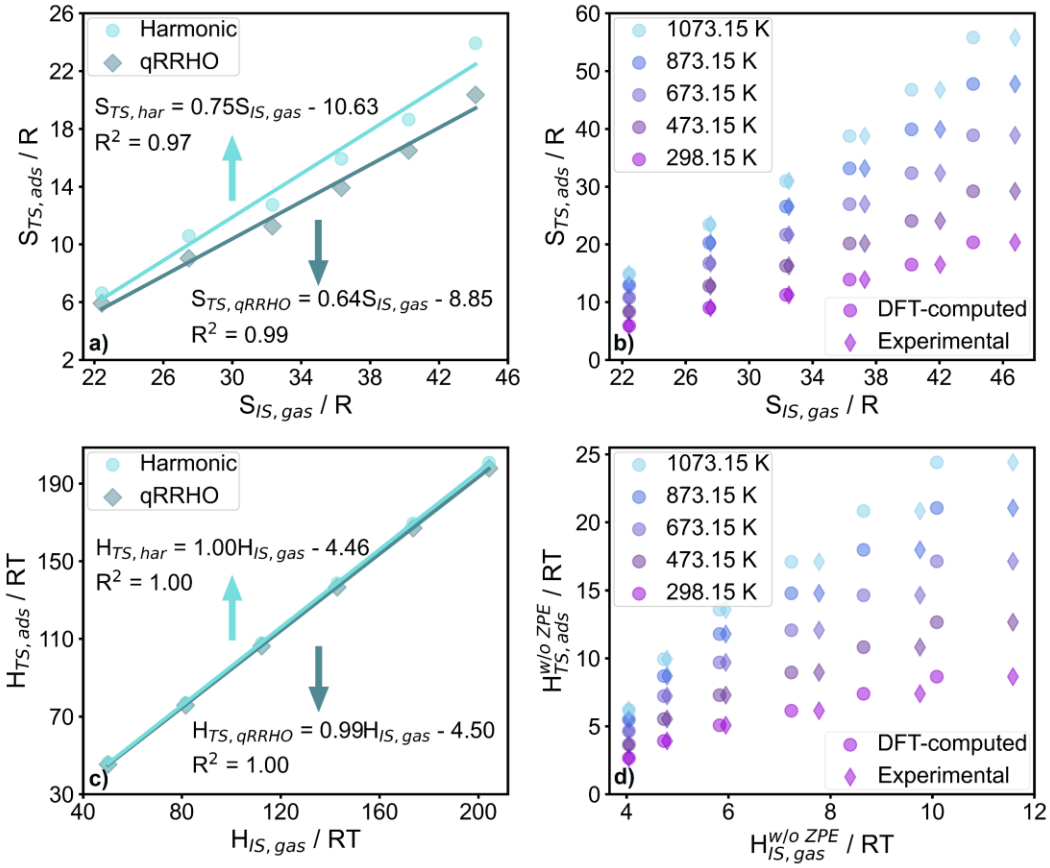

Figure 2. (a) Entropic and **(c)** enthalpic scaling of transition states (TSs) on Pt(111) surfaces against initial states (ISs) in the gas phase. Entropies and enthalpies for transition states ($S_{TS,ads}$, $H_{TS,ads}$) are calculated using the harmonic approximation (circles) or the quasi-rigid rotor harmonic oscillator (qRRHO) approximation (diamonds). Thermochemical quantities are calculated at 298.15 K. Slopes, y-intercepts, and fits are rounded to two decimal places for brevity. Comparison for **(b)** entropies and **(d)** enthalpic corrections using either DFT-computed or experimental references for gas-phase thermochemistry at 298.15 K (x-axis) and DFT-data for transition state calculations (qRRHO) at 5 temperatures (y-axis). Note that the gas-phase enthalpic corrections in **(d)** do not include ZPE terms, or include temperature corrections only.

Incorporating bond-breaking (or forming) TS complexes into thermochemical scaling relationships may prove especially beneficial for avoiding expensive DFT computations. Figure 2a and 2c shows the entropic and enthalpic corrections, respectively, at the TS of C_1-C_6 dehydrogenation reactions,

$$C_nH_{2n+2}{}^* \ (physisorbed) \rightarrow \ C_nH_{2n+1}{}^* \ + H^*, \qquad 11$$

on Pt(111) surfaces against those of the corresponding thermochemical quantities of C_1-C_6 gas-phase alkanes. The terminal -CH_3 bond is dehydrogenated for all alkanes, and only this single TS structure across C-H bond scissions is considered. Strong linear correlations among the TS thermochemical relations are presented; given the TS calculations are performed on the same metal, with the same surfaces sites chosen for the initial and final states, the geometries of the TS structures in relation to positions over the surface are similar are well. For the same dataset, Figure S3a in the SI shows scaling of Gibbs energies at the TS against gas-phase species can also be constructed.

Thermochemical scaling relationships presented thus far have been constructed solely based on DFT data; it may also be advantageous to consider a hybrid of DFT and experimental results when correlating properties. Figure 2b and 2d show using either DFT or experimental gas-phase references for thermochemical properties, where experimental values are obtained from NIST.[29] In Figure 2d the enthalpy difference relative to absolute zero is plotted, or ZPE terms are not included. Notably, as the molecule size increases, DFT-computed gas-phase thermochemistry is underestimated compared to experimental values as attributed to the inaccuracies of the harmonic approximation.[7] Further, deviations from experimental values may be due to insufficient assessment of internal rotational contributions,[35] or exclusion of the conformational entropy which becomes more important with greater flexibility of the molecule.[36] While the regressions will differ, both DFT and experimental references may be used to construct thermochemical relations.

To further elaborate on possible admonitions of using the harmonic approximation, the model introduces sources of error for DFT computation of adsorbate-surface frequencies, notably the neglect of anharmonicities. Specifically, low-frequency modes contribute largely to entropies, and potentially significant frustrated rotational and translational motions may be inaccurately assessed and can lead to errors in the pre-exponential factor. A number of methodologies have been developed to overcome harmonic approximation limitations for low-frequency modes; for example, Campbell et al. proposed hindered translator and rotor models for treating the lowest frequency modes of surface species.[37, 38] Hindered translational / rotational treatment requires careful examination of normal modes, which must have sinusoidal potentials. Sauer et al. proposed independent sampling of normal modes transformed into curvilinear internal coordinates to obtain anharmonic potentials,[39, 40] and extended the anharmonic approach to rigid body coordinates to avoid complications in defining a set of internal coordinates for adsorbate-surface systems.[41] Madix and coworkers further quantified the effect of hindered rotor corrections on the pre-exponential.[42] For a homologous series of alkoxides, pre-exponentials for dehydrogenation reactions on a Cu(110) surface were calculated with the harmonic approximation only or were determined by treating the lowest frequency frustrated rotation in the reactant state as a hindered rotor. It was found that the hindered rotor correction to the pre-exponential becomes larger with increasing molecular size, with a correction factor q_{rot}/q_{har} of ~3 at 300 K for the largest alkoxy studied, 1-butoxy. For larger species that are relatively uninhibited on a surface, frustrated periodic rotations become more significant.[42] We then expect anharmonic corrections to become more important when predicting entropies of successively larger species in the homologous series of alkyls defined in this work. Further, other frustrated rotations and translations without periodic angular potentials may also contribute to significant changes in the pre-exponential, and motions at the TS may be constrained due to geometric orientation relative to the surface or they may be entropically mobile. Attempting to decouple and manually identify normal modes that should be treated as frustrated motions or anharmonicities is a laborious task. For computing enthalpic corrections, anharmonic treatment of high-frequency modes become important, such as for stretching motions of hydrogen-bonded OH groups.[43] While anharmonic and experimentally observed stretching frequencies have been linearly related to harmonic wavenumbers, empirical corrections may be inadequate to describe systems with substantial hydrogen bonding.[43] In this work, we only address the basic treatment of frequencies using the harmonic approximation and a "black-box" extension through the qRRHO model to alleviate any numerical

noise in low-lying surface vibrations.[30] Both models demonstrate strong linear regressions in the proposed thermochemical correlations; however, future work should assess the effect of anharmonicities on such scaling relations, as they may have a substantial impact on the thermochemistry and quantities such as the pre-exponential.

It is also worthy to note the (appeared) linearity of the entropic and enthalpic correlations with ZPE terms compared to the logarithmic nature of Figure 2d. ZPE terms comprise a majority of enthalpic corrections, and the overall regressions are dictated by this. Figure S3b in the SI demonstrates scaling of ZPE terms only. Isolating temperature corrections is an example of examining nonlinearities in separate contributions to thermochemical quantities. Interestingly, entropic correlations appear linear in nature while containing several dependencies on nonlinear partition functions, and the next section further examines why this occurs.

Entropic Scaling Depends on Construction of the Homologous Series

Examining fundamental aspects behind thermochemical scaling provides greater insight into when and how these relationships may be applied. Figure 3a shows the ratio of adsorbed entropy / gas-phase entropy for gas-phase species A and dehydrogenated surface species A* on Pt(111) as shown in Tables S1 and S2 of the SI. The adsorbed entropic component becomes larger relative to the gas-phase one with increasing size, due to the relationship of the partition functions with the size of the molecule. Table S3 in the SI shows that for gas-phase entropies as the carbon number increases the vibrational contribution

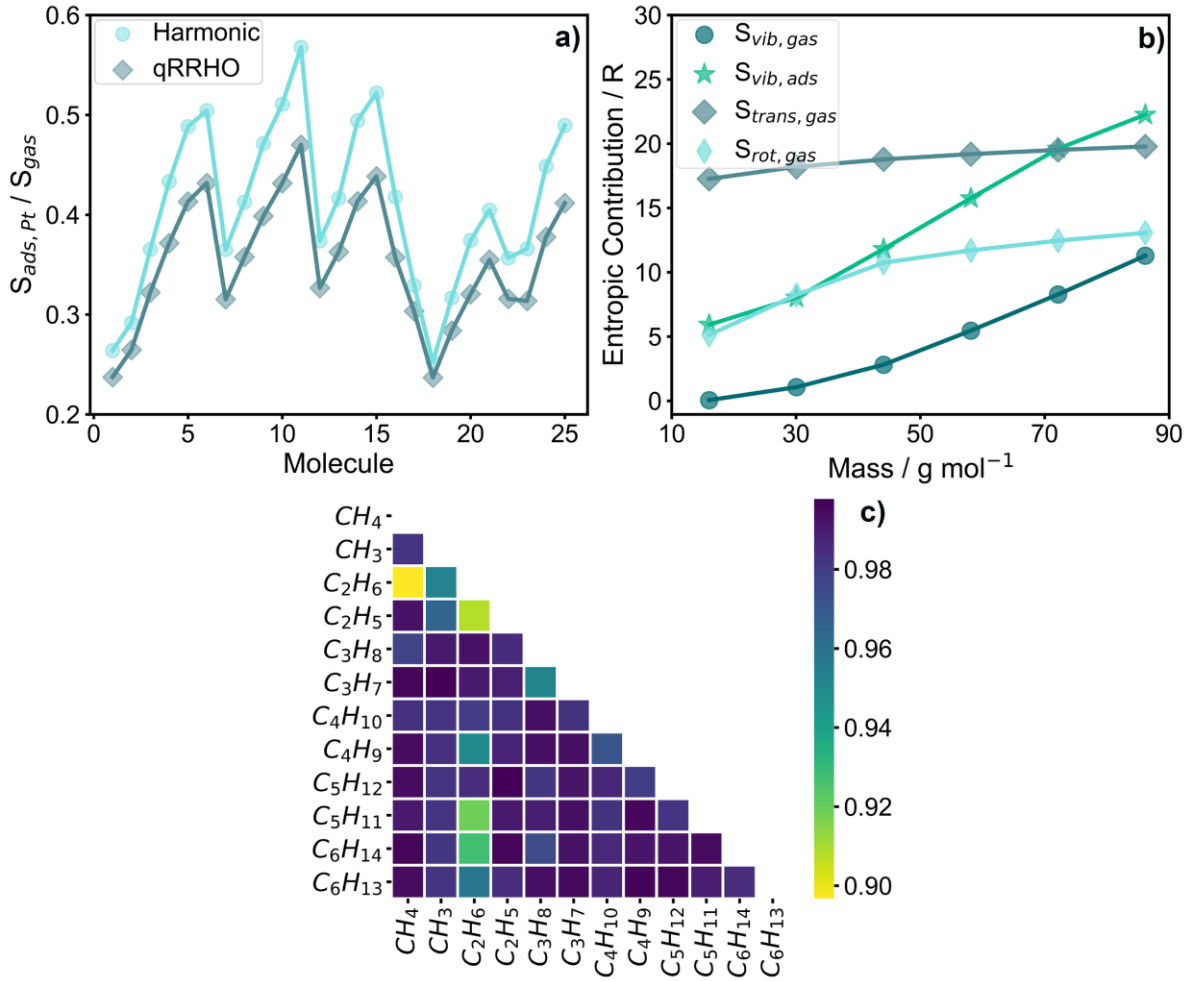

Figure 3. **(a)** Ratio of adsorbate/gas-phase species entropy for every molecule pairing of gas-phase species A and dehydrogenated surface species A* on Pt(111) in Tables S1 and S2 of the SI (numbered arbitrarily as integers). **(b)** Entropic contributions for gas-phase and adsorbed molecules plotted against molar mass of hydrocarbons. Gas-phase species entropic contributions are calculated for C_1-C_6 alkanes and adsorbate contributions for C_1-C_6 alkyls adsorbed on Pt(111). **(c)** Heat map of Pearson correlation coefficients comparing entropic contributions from individual vibrational modes for C_1-C_6 gas-phase alkanes/alkyl chains adsorbed on Pt(111). Given the number of individual entropic contributions are different lengths for different molecules (i.e. depending on the vibrational degrees of freedom of the molecule), the correlation coefficients are calculated from rolling correlations where all possible configurations are mapped from a larger to a smaller array, and the highest coefficient is taken. The high correlation coefficients signify that individual vibrational entropic contributions among the studied molecules are highly linearly related to each other across and between gas-phase/adsorbed species. For **(b)** and **(c),** vibrational entropic contributions are calculated using the harmonic oscillator model.

becomes proportionally a larger component of the total entropy, even as all partitional components increase. We show that individual vibrational entropic contributions are linearly correlated with each other in Figure 3c, where the heatmap indicates high correlation coefficients between gas-phase and adsorbed hydrocarbons. In all, piecewise vibrational contributions become more important for both gas-phase and adsorbed molecules with increasing size.

As noted, these linear relations are dependent on the successive increase in the size, or chain length, of the molecule. By this, we define size as related to mass (affecting S_{trans} and S_{rot} terms) and the degrees of freedom (affecting S_{vib} terms). Figure 3b plots entropic contributions of the translational, rotational, and vibrational partition functions against molar mass. As the molar mass increases, all partitional components increase; the translational entropy is directly dependent on the mass of the molecule (Equation 1), while the rotational entropy contains the moments of inertia (Equation 2), which depend on the masses and coordinates of the atoms.[44] The vibrational entropy always increases as the number of atoms in the defined (long-chain hydrocarbon) homologous series increases, since the term is a summation of (always positive) entropic contributions over the vibrational degrees of freedom in the species (Equation 3). Both the translational and rotational entropies follow a logarithmic trend, while the vibrational components for both gas and adsorbed species are linear in nature. For gas-phase species, the vibrational entropy approaches a limit of zero as the molar mass becomes smaller, as the vibrational contribution must be positive for species with two atoms or more. For molecules with lower molar mass, the translational and rotational components contribute the most to the gas-phase entropy, but as the size of the molecule increases, the vibrational component becomes nearly as large as the rotational one; with increasing hydrocarbon chain length, the vibrational partition function would surpass the rotational and translational contributions to the total entropy. Essentially, then, entropic scaling relationships are driven by the change in vibrational entropy as the size of the molecule, and therefore the degrees of freedom, increases.

While the trends in Figure 3b appear logarithmic for translational and rotational contributions and linear for vibrational contributions, further justification and insights regarding the linearity (or lack thereof) of such partition functions are important. Supplementary Note S1 details first-order Taylor series expansions of each entropic component, where we determine if entropic contributions as a function of size may be approximated as linear or not. As previously discussed, the vibrational entropy successively increases for the defined homologous series as the vibrational degrees of freedom increase. The Taylor series expansion around a reference frequency for the vibrational entropy validates how individual vibrational frequencies are linearly correlated between different alkanes/alkyl chains, thus establishing the linearity of thermochemical scaling relationships. Most frequencies calculated from the Taylor expansion match well with those determined from the statistical thermodynamic equation (with some scatter); this is especially important for lower frequencies which contribute proportionally to larger entropic terms.

Integrating Thermochemical Scaling Relationships with Microkinetic Models

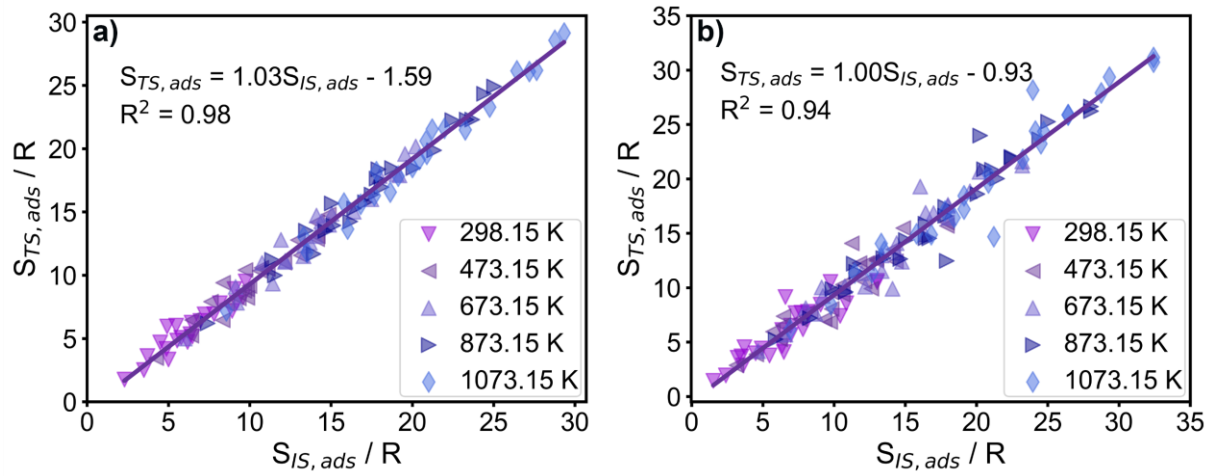

Figure 4. Entropies of **(a)** C-C and **(b)** C-H bond scission reactions for propane and ethane hydrogenolysis at transition states (TSs) against initial states (ISs) on Ru(0001). Entropies for adsorbed species (S_{ads}) are calculated using the quasi-rigid rotor harmonic oscillator (qRRHO) approximation at 5 different temperatures.

To demonstrate practical applicability of thermochemical correlations, we developed linear relations to predict entropic contributions at TSs for pre-exponential factors (A) of elementary reactions in propane and ethane hydrogenolysis.[32] To circumvent DFT computations, an approximation of the pre-exponential as calculated by TS theory is made by neglecting entropies, or using $\frac{k_b T}{h}$; thermochemical correlations would instead allow for the estimation of entropies while avoiding expensive DFT calculations. We plot the TS entropy against that of the IS for 23 C-C and 26 C-H bond-breaking reactions in Figure 4. The elementary steps are listed in Table S4 of the SI. Correlating TSs to radical species in the gas-phase would require incorporation of the electronic partition function, where thermochemical scaling relations would no longer hold. Generally, as the entropy of the IS increases, the entropy of the TS also increases. However, when constructing these relations for a single temperature, there is more scatter across entropic scaling for propane and ethane hydrogenolysis. Given that entropies for both C-H and C-C bond scissions scale with a slope close to 1 and small y-intercepts, this may be indicative of other bond breaking reactions such as C-O, N-H, C-N, etc. also scaling with a similar trend.

Figure S4a and S4c in the SI show that the entropic scaling relationships can be constructed with either the IS or FS correlated with the TS across C-C and C-H bond scissions, analogous to how a TSS relation would be constructed for energetics. Figure S4b and S4d demonstrate how a BEP-like relationship for entropies would be constructed for C-C and C-H bond scissions, respectively. For C-C bond scissions, the BEP-like relation is quite scattered, while for C-H bond scissions, the correlation has a better fit. Overall, though, the fits for the BEP-like entropic relations are worse than those for the TSS-like relations. The TSS-like relations have a larger span of entropies covered (due to the range of molecule size), but the BEP-like relations cancel this size effect.

Figure S5a in the SI shows a parity plot between the DFT-obtained entropy at the TS and the entropy predicted using the linear regressions in Figure 4 for elementary reactions in propane and ethane hydrogenolysis. Predicted values are generally close to those obtained from DFT-data; however, even minor

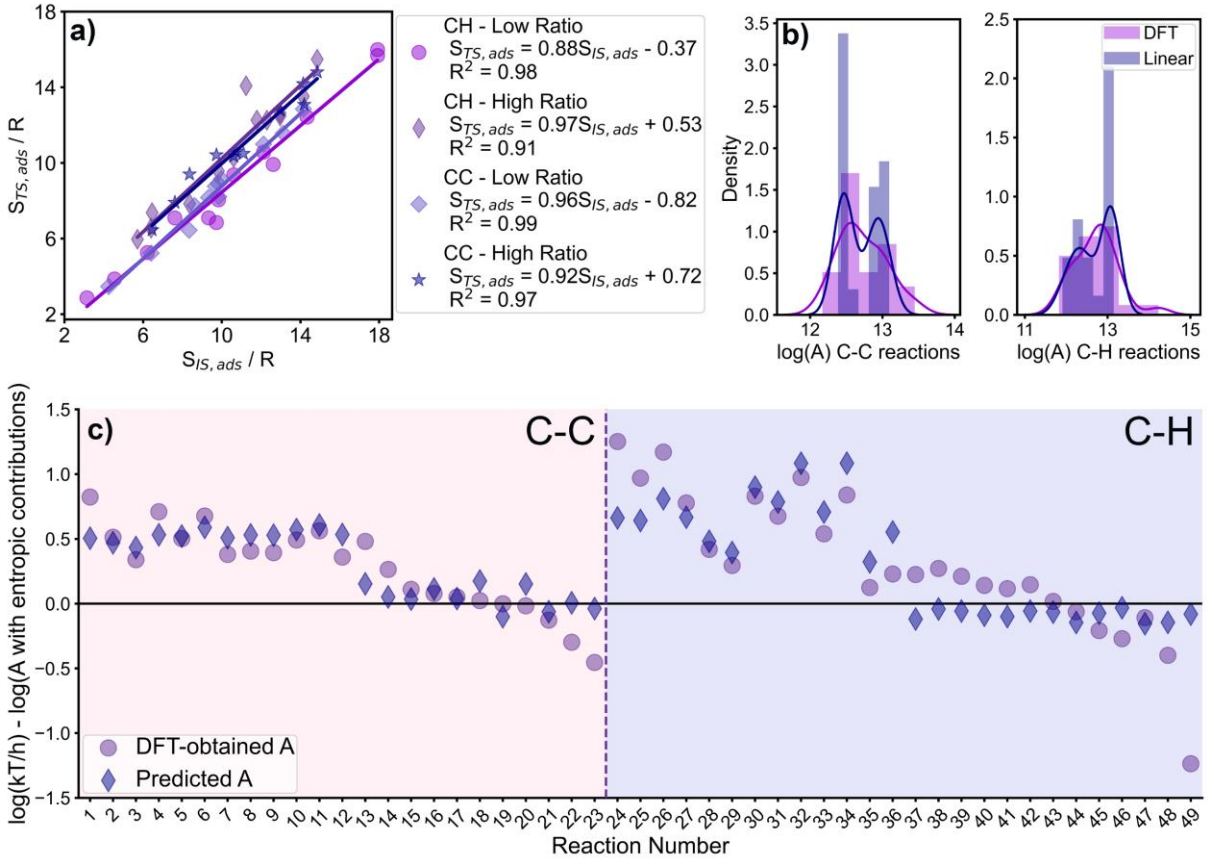

Figure 5. **(a)** Entropies of C-H and C-C bond scission reactions for propane and ethane hydrogenolysis at transition states against initial states on Ru(0001). Entropies for adsorbed species (S_{ads}) are calculated using the quasi-rigid rotor harmonic oscillator (qRRHO) approximation. Linear regressions are classified by the ratio of the partition functions at the transition state / initial state for both C-C and C-H reactions. **(b)** Distribution of pre-exponentials (A) for C-C and C-H bond scissions at 473.15 K calculated using either DFT data or linear regressions from Figure 5a. A kernel density estimate is used for smoothing observations and approximating the underlying probability density function. **(c)** Difference between the log of $\frac{k_b T}{h}$ and the log of the pre-exponential (A) computed using entropic contributions either obtained from exact DFT data or from the linear regressions in Figure 5a. The reactions numbers are arbitrarily named as integers except to distinguish between C-C and C-H reactions; reactions 1-23 are C-C bond scissions and reactions 24-49 are C-H bond scissions. Pre-exponentials are in units of s^{-1}.

errors in prediction have a considerable effect on obtaining accurate estimates for certain pre-exponentials. Figure S5b in the SI shows the difference between using the approximation of $\frac{k_b T}{h}$ and including entropic contributions in the pre-exponential term, either through DFT-obtained data or using linear correlations. While many linear regression predictions lie within a half an order-of-magnitude of the exact DFT data, there are a number of predictions that do not capture outlying pre-exponentials. Most elementary reactions in propane and ethane hydrogenolysis have relatively similar entropic contributions between transition and initial states (or the ratio of their respective partition functions is nearly 1); as linear regressions only capture the mean of the dependent variable, elementary reactions with significant changes between entropies of local minima and TSs are severely over/under-estimated by the scaling relationships.

To obtain better estimates of the entropic contributions at the TS, we further classified the C-H and C-C bond-breaking DFT datasets by grouping data based on the ratios of partition functions. Figure 5a demonstrates this breakdown of C-H and C-C datasets, but it requires prior knowledge of when a reaction is likely to yield larger differences between the IS and TS partition functions. Generally, the modified scaling relations in Figure 5a demonstrate improvement in capturing outlying trends. Figure 5b shows the distribution of the log of pre-exponentials for DFT-calculated and predicted values. For DFT-calculated values, distributions appear more unimodal in nature while pre-exponentials predicted using linear regressions demonstrate more bimodal inclinations. Given the breakdown of C-C and C-H bond scission data into two subsets based on partition functions, it would make sense that linear predictions would follow bimodal tendencies. Figure S6 in the SI shows the distribution of errors between using $\frac{k_b T}{h}$ versus linear predictions or exact DFT data for entropic contributions. Figure 5c plots the error between the $\frac{k_b T}{h}$ approximation with pre-exponentials calculated from either DFT data or estimated using entropic correlations from Figure 5a. Pre-exponentials that vary by more than half an order of magnitude from $\frac{k_b T}{h}$ show pronounced improvement in predictions. Notably, these reactions can be classified as certain subgroups of C-C or C-H datasets; for C-H bond-breaking reactions, the initial dehydrogenation of physisorbed species such as CH_4 (Reaction 26), C_2H_6 (Reaction 30), and C_3H_8 (Reactions 32 and 34) all show large deviation from $\frac{k_b T}{h}$, where pre-exponentials are ~0.75 or more orders of magnitude lower than 10^{13}. Additionally, intermediate C-H dehydrogenation steps where -CH_3 groups lose a hydrogen will diverge from $\frac{k_b T}{h}$. This includes elementary steps $CH_3C^* + * \rightarrow CH_2C^* + H^*$ (Reaction 25), $CH_3CH^* + * \rightarrow CH_2CH^* + H^*$ (Reaction 27), $CH_3CCH^* + * \rightarrow CH_2CCH^* + H^*$ (Reaction 31), and $CH_3CH_2^* + * \rightarrow CH_2CH_2^* + H^*$ (Reaction 33). Some outlying elementary steps exist, such as $CH_2CH^* + * \rightarrow CHCH^* + H^*$ (Reaction 24), which is 1.25 orders of magnitude lower than 10^{13}, and $CH_3CH_2CH_2^* + * \rightarrow CH_3CH\text{-}_2CH^* + H^*$ (Reaction 49), which is 1.25 orders of magnitude higher than 10^{13}. We describe below using exact DFT data, entropic scaling relationships classified by partition function ratios, and a hybrid of the two methods to obtain pre-exponentials for propane and ethane hydrogenolysis. Depending on the kinetically relevant step(s) in a MKM, entropic contributions may significantly change outputs.

Table 1. MKM results for ethane and propane hydrogenolysis on Ru(0001) using a plug flow reactor. Each testing condition is as follows: 1) no entropic contributions are included in the pre-exponential term ($\frac{k_b T}{h}$ only), 2) entropic contributions are estimated from the thermochemical scaling relations in Figure 5, and 3) entropic contributions are calculated from exact DFT data. **In the case of propane hydrogenolysis, test condition 3 is a combination of exact DFT data and estimates from thermochemical scaling relations. For ethane hydrogenolysis, kinetic signatures measured at $P(C_2H_6)$ = 0.03 atm, $P(H_2)$ = 0.20 atm, and T = 478 K. For propane hydrogenolysis, kinetic signatures measured at $P(C_3H_8)$ = 0.03 atm, $P(H_2)$ = 0.20 atm, T = 433 K.

Ethane Hydrogenolysis			Propane Hydrogenolysis		
Microkinetic Model Test	TOF (s^{-1})	Conversion (%)	Microkinetic Model Test	TOF (s^{-1})	Conversion (%)
1	5.4×10^{-5}	4.37	1	5.1×10^{-4}	37.68
2	1.8×10^{-5}	1.43	2	6.7×10^{-5}	4.99
3	1.1×10^{-5}	0.92	3	8.3×10^{-5}	6.17

Table 1 shows MKM results comparing the $\frac{k_b T}{h}$ approximation, exact DFT data, and linear regressions. Incorporation of entropic contributions into the two reaction networks studied has variable

effects on MKM outputs such as turnover frequency (TOF) and conversion, depending on kinetically relevant steps of the dominant catalytic pathway. While the neglect of anharmonic corrections may introduce errors in DFT-computed entropies, and hence the MKM, our objective is to reproduce 'exact' DFT calculations using thermochemical scaling relationships. Additionally, several input parameters can affect MKM results, so the presented example is considered as a self-contained case study examining entropic effects on pre-exponentials only.

For ethane hydrogenolysis, MKM results are similar between using $\frac{k_b T}{h}$ and incorporating entropic contributions. The CHCH* C-C bond scission is the rate determining step (RDS) and *A* is on the same order-of-magnitude. The DOF lost at the TS is not a low-lying (generally < 100 cm^{-1}) vibrational mode, and the partition functions/entropies are similar between the TS and IS, so the $\exp\left(\frac{\Delta S^{\ddagger}}{R}\right)$ term is close to unity.

For propane hydrogenolysis, there are 121 elementary reactions in the catalytic cycle; since DFT data was not available for all steps and was computationally prohibitive to calculate, a hybrid of exact DFT and scaling relations was used to determine entropic contributions. In a similar fashion to a TSS/BEP, a thermochemical scaling relationship for a large reaction network may first be constructed using select DFT-obtained data, and then applied to other reactions such that thermochemical properties may be estimated. Relative to the ethane hydrogenolysis case, MKM results show greater differentiation between the $\frac{k_b T}{h}$ approximation and including entropic contributions. The RDS is the first dehydrogenation step of physisorbed C_3H_8* + * → $CH_3CH_2CH_2$* + H* for all testing conditions, where we would expect to observe notable differences between entropies at the IS and TS. For reactions like dehydrogenations of physisorbed molecules, certain degrees of freedom of the reactant are very unstable and there is a weak association between the molecule and the surface.[14] At the TS a larger component of the adsorbate becomes attached to the surface (i.e. the dissociating propyl-hydrogen complex) so the loss of particularly low-lying degrees of freedom causes the partition function at the TS to be much lower than that of the IS, hence the significant difference in the pre-exponential. Although a general trend between the partition functions of the reactant and TS can be elucidated, we note the harmonic approximation does not consider frustrated rotational and translational motions, and future work should focus on establishing scaling relations that incorporate anharmonic effects.

MKMs may be refined using the hierarchical approach, where postulated models are improved using DFT-obtained data; with the aim of reduced computational cost, DFT calculations for kinetically relevant steps are performed until consistent reaction mechanisms are achieved between successive iterations.[45] In previous work, we found that while qualitatively correct MKMs for ethanol steam reforming could be achieved with minimal refinement of initial parameters, quantitative models required additional refinement of thermochemistry for determining species free energies and activation free energies.[45] The scaling relationships presented in this work can similarly aid in reducing computational cost while achieving similar results to an 'exact' DFT-based model. The hierarchical methodology is sufficient to use in the presented case study of propane/ethane hydrogenolysis on Ru(0001),[32] where pre-exponentials for kinetically relevant steps are calculated in secondary refinement. However, in a hypothetical case there may be misidentification of a kinetically relevant step using the hierarchical approach if pre-exponentials from DFT-obtained data are several orders-of-magnitude off from the initial $\frac{k_b T}{h}$ approximation. It is then useful to consider initial estimation of pre-exponentials using scaling relationships if DFT data is unavailable for all elementary steps to gauge whether entropic contributions may have a significant impact on MKM results.

Conclusions

In this work, we first examined thermochemical scaling relations between C_1-C_6 *n*-alkanes in the gas-phase and adsorbed alkyl chains extending from a metal surface, and subsequently added functional groups such as -OH, -NH_2, C=O, and C=C. We found strong linear correlations between gas-phase and adsorbed species and showed thermochemical scaling relationships depend on the choice of a given homologous series; in the examples presented, linearity is dependent on successively increasing hydrocarbon chain length. We extended the correlations to incorporate TSs of dehydrogenation reactions, allowing for quick estimation of thermochemistry. Moreover, we rationalized the linearity of thermochemical correlations based on statistical mechanical fundamentals and the construction of the homologous series. As an application, we demonstrated estimation of the pre-exponential for elementary surface reactions of ethane and propane hydrogenolysis on Ru(0001). Depending on the dominant catalytic pathway and the RDS, inclusion of entropic contributions has variable effects on kinetic outcomes. For the RDS of ethane hydrogenolysis, the ratio of TS:IS partition functions is closer to unity, and entropic effects are negligible. In contrast, the RDS of propane hydrogenolysis has a labile IS and stabilized TS, so entropic effects become more important. Ideally, DFT data would be readily available for all elementary steps in a MKM, but in computationally unviable cases we recommend that thermochemical parameters are at least estimated with linear correlations.

An important caveat of the proposed thermochemical scaling relationships is neglected anharmonicities. Potential directions for future work should include frustrated translational and rotational corrections to low-frequency modes and exploration of the propagated effects on kinetic signatures. Additionally, while most of the (predicted) thermochemical quantities in this work are for reaction intermediates and transition states, similar relations can be constructed for other homologous series. Experimental bond energies for certain adsorbed intermediates have already been gathered,[46] and the validity of the thermochemical relations could be verified against DFT-computed corrections to experimental adsorption enthalpies.[47]

Author Contributions

Sophia Kurdziel: Conceptualization, Methodology, Formal analysis, Visualization, Writing – Original Draft, Writing – Review & Editing. **Dionisios Vlachos**: Conceptualization, Writing – Review & Editing, Funding acquisition.

Conflicts of Interest

There are no conflicts of interest to declare.

Data Availability

VASP output files describing geometries, as well as an Excel file that contains energies and thermochemistry calculated from DFT used in generating the figures contained in this work are available on Zenodo at https://zenodo.org/record/7493083#.Y68epXbMJPZ. Other data will be provided by the corresponding author upon reasonable request.

Supporting Information

Supplementary data associated with this article can be found in the online version at DOI:

Acknowledgements

Financial support from the RAPID manufacturing institute, supported by the Department of Energy (DOE) Advanced Manufacturing Office (AMO), award number DE-EE0007888-9.5 is gratefully acknowledged. RAPID projects at the University of Delaware are also made possible in part by funding provided by the State of Delaware. The Delaware Energy Institute gratefully acknowledges the support and partnership of the State of Delaware in furthering the essential scientific research being conducted through the RAPID projects. This research was supported in part through the use of Information Technologies (IT) resources at the University of Delaware, specifically the high-performance computing resources. The authors also acknowledge useful discussions with Dr. Gerhard Wittreich.

References

1. F. Abild-Pedersen, J. Greeley, F. Studt, J. Rossmeisl, T. R. Munter, P. G. Moses, E. Skulason, T. Bligaard and J. K. Nørskov, *Phys. Rev. Lett.*, 2007, **99**, 016105.
2. S. Wang, V. Petzold, V. Tripkovic, J. Kleis, J. G. Howalt, E. Skúlason, E. M. Fernández, B. Hvolbæk, G. Jones, A. Toftelund, H. Falsig, M. Björketun, F. Studt, F. Abild-Pedersen, J. Rossmeisl, J. K. Nørskov and T. Bligaard, *Phys. Chem. Chem. Phys.*, 2011, **13**, 20760-20765.
3. A. U. Nilekar, J. Greeley and M. Mavrikakis, *Angew. Chem. Int. Ed. Engl.*, 2006, **45**, 7046-7049.
4. J. L. Lansford, A. V. Mironenko and D. G. Vlachos, *Nat. Commun.*, 2017, **8**, 1842.
5. J. L. Lansford, S. J. Kurdziel and D. G. Vlachos, *J. Phys. Chem. C*, 2021, **125**, 7119-7129.
6. S. J. Kurdziel, J. L. Lansford and D. G. Vlachos, *J. Phys. Chem. C*, 2021, **125**, 19780-19790.
7. C. T. Campbell and J. R. V. Sellers, *J. Am. Chem. Soc.*, 2012, **134**, 18109-18115.
8. C. T. Campbell and J. R. V. Sellers, *Chem. Rev.*, 2013, **113**, 4106-4135.
9. A. Budi, S. L. S. Stipp and M. P. Andersson, *J. Phys. Chem. C*, 2018, **122**, 8236-8243.
10. P. J. Dauenhauer and O. A. Abdelrahman, *ACS Cent. Sci.*, 2018, **4**, 1235-1243.
11. C. Rzepa, D. W. Siderius, H. W. Hatch, V. K. Shen, S. Rangarajan and J. Mittal, *J. Phys. Chem. C*, 2020, **124**, 16350-16361.
12. B. A. De Moor, M.-F. Reyniers, O. C. Gobin, J. A. Lercher and G. B. Marin, *J. Phys. Chem. C*, 2011, **115**, 1204-1219.
13. K. C. Waugh, *Catal. Today*, 1999, **53**, 161-176.
14. C. T. Campbell, Y. K. Sun and W. H. Weinberg, *Chem. Phys. Lett.*, 1991, **179**, 53-57.
15. S. Deshmukh, A. Mhadeshwar and D. Vlachos, *Am. Chem. Soc. Div. Fuel Chem. Prepr.*, 2003, **48**.
16. A. Nigam and M. T. Klein, *Ind. Eng. Chem. Res.*, 1993, **32**, 1297-1303.
17. L. J. Broadbelt, S. M. Stark and M. T. Klein, *Ind. Eng. Chem. Res.*, 1994, **33**, 790-799.
18. G. Kresse and J. Furthmüller, *Phys. Rev. B*, 1996, **54**, 11169-11186.
19. A. Hjorth Larsen, J. Jørgen Mortensen, J. Blomqvist, I. E. Castelli, R. Christensen, M. Dułak, J. Friis, M. N. Groves, B. Hammer, C. Hargus, E. D. Hermes, P. C. Jennings, P. Bjerre Jensen, J. Kermode, J. R. Kitchin, E. Leonhard Kolsbjerg, J. Kubal, K. Kaasbjerg, S. Lysgaard, J. Bergmann Maronsson, T. Maxson, T. Olsen, L. Pastewka, A. Peterson, C. Rostgaard, J. Schiøtz, O. Schütt, M. Strange, K. S. Thygesen, T. Vegge, L. Vilhelmsen, M. Walter, Z. Zeng and K. W. Jacobsen, *J. Phys. Condens. Matter*, 2017, **29**, 273002.
20. B. Hammer, L. B. Hansen and J. K. Nørskov, *Phys. Rev. B*, 1999, **59**, 7413-7421.
21. S. Grimme, J. Antony, S. Ehrlich and H. Krieg, *J. Chem. Phys.*, 2010, **132**, 154104.
22. G. Kresse and D. Joubert, *Phys. Rev. B*, 1999, **59**, 1758-1775.
23. H. J. Monkhorst and J. D. Pack, *Phys. Rev. B*, 1976, **13**, 5188-5192.
24. R. T. Downs and M. Hall-Wallace, *Am. Mineral.*, 2003, **88**, 247-250.
25. G. Henkelman, B. P. Uberuaga and H. Jónsson, *J. Chem. Phys.*, 2000, **113**, 9901-9904.
26. G. Henkelman and H. Jónsson, *J. Chem. Phys.*, 1999, **111**, 7010-7022.
27. B. C. Bukowski, J. S. Bates, R. Gounder and J. Greeley, *J. Catal.*, 2018, **365**, 261-276.

28. D. A. McQuarrie, *Statistical mechanics*, University Science Books, Sausalito, Calif., 2000.
29. NIST Computational Chemistry Comparison and Benchmark Database, NIST Standard Reference Database Number 101, http://cccbdb.nist.gov/, (accessed September 2022).
30. S. Grimme, *Chem. Eur. J*, 2012, **18**, 9955-9964.
31. Y.-P. Li, J. Gomes, S. Mallikarjun Sharada, A. T. Bell and M. Head-Gordon, *J. Phys. Chem. C*, 2015, **119**, 1840-1850.
32. T. Xie, G. R. Wittreich and D. G. Vlachos, *Appl. Catal. B*, 2022, **316**, 121597.
33. M. E. Coltrin, R. J. Kee and F. M. Rupley, *Int. J. Chem. Kinet.*, 1991, **23**, 1111-1128.
34. A. Michaelides and P. Hu, *J. Chem. Phys.*, 2001, **114**, 2523-2526.
35. J. M. Hudzik and J. W. Bozzelli, *Adv. Phys. Chem.*, 2013, **2013**, 673065.
36. P. Pracht and S. Grimme, *Chem. Sci.*, 2021, **12**, 6551-6568.
37. L. H. Sprowl, C. T. Campbell and L. Árnadóttir, *J. Phys. Chem. C*, 2016, **120**, 9719-9731.
38. C. T. Campbell, L. H. Sprowl and L. Árnadóttir, *J. Phys. Chem. C*, 2016, **120**, 10283-10297.
39. G. Piccini and J. Sauer, *J. Chem. Theory Comput.*, 2013, **9**, 5038-5045.
40. G. Piccini and J. Sauer, *J. Chem. Theory Comput.*, 2014, **10**, 2479-2487.
41. M. Rybicki and J. Sauer, *J. Chem. Theory Comput.*, 2022, **18**, 5618-5635.
42. W. Chen, L. Sun, B. Kozinsky, C. M. Friend, E. Kaxiras, P. Sautet and R. J. Madix, *J. Phys. Chem. C*, 2020, **124**, 1429-1437.
43. J. Spanget-Larsen, B. K. V. Hansen and P. E. Hansen, *Chem. Phys.*, 2011, **389**, 107-115.
44. U. Ryde, *MedChemComm*, 2014, **5**, 1324-1336.
45. J. E. Sutton and D. G. Vlachos, *Chem. Eng. Sci.*, 2015, **121**, 190-199.
46. C. T. Campbell, *Acc. Chem. Res.*, 2019, **52**, 984-993.
47. J. Wellendorff, T. L. Silbaugh, D. Garcia-Pintos, J. K. Nørskov, T. Bligaard, F. Studt and C. T. Campbell, *Surf. Sci.*, 2015, **640**, 36-44.